Optical properties and photocatalytic performance of

Si/TiO₂ tandem semiconductor microwire slurries

Saumya Gulati, Matthew C. Mulvehill, Tyler C. Thompson, and Joshua M. Spurgeon*

Conn Center for Renewable Energy Research, University of Louisville, Louisville, Kentucky,

40292, USA.

*E-mail: joshua.spurgeon@louisville.edu

KEYWORDS. slurry, solar fuel, tandem, microwire, photocatalysis, water-splitting

ABSTRACT

Semiconductor particle suspension reactors hold promise as a possible low-cost strategy for solar

water-splitting, but they face several challenges that have inhibited their solar-to-hydrogen

(STH) efficiencies. A tandem microparticle with a buried junction addresses some of these

challenges and offers a pathway to high STH efficiency. As a slurry, the tandem microparticles

need to be suspended and well-dispersed with maximum light absorption for a minimal

photoactive particle concentration. Herein, proof-of-concept Ni/np⁺-Si/FTO/TiO₂ tandem

microwire structures capable of unassisted solar water-splitting were investigated as a slurry

1

using uplifting N₂ carrier gas bubbles. Transmittance, reflectance, and absorptance of the slurry were characterized as a function of wavelength, bubble flowrate, and tandem microwire concentration using an integrating sphere. Notably, a slurry absorptance of 70 – 85% was achieved with only 1% of the solution volume filled with photoactive material. Photochemical activity of the slurry was characterized with in-situ monitoring of the photodegradation of methylene blue, including the effects of particle concentration, bubble flowrate, spectral mismatch, intermixed light scattering particles, and a back reflector.

INTRODUCTION

Hydrogen has the potential to be a clean alternative to fossil fuels, and H₂ synthesis from water electrolysis is an ideal, highly scalable, and energy-dense way to store the energy from intermittent power generation sources. The present predominant industrial method of H₂ production via steam methane reforming (SMR) from natural gas produces large amounts of greenhouse gas CO₂ emissions. With the urgent need to shift society from fossil fuels to a cleaner alternative, extensive research has been directed towards renewably produced, or green, hydrogen. In the most straightforward route, efficiently coupled photovoltaic (PV) + electrolyzer technologies have yielded solar hydrogen from water splitting at high solar-to-hydrogen (STH) efficiencies.¹⁻³ However, this approach has been far from cost-competitive with hydrogen produced by SMR.^{4, 5} An alternative solar water-splitting reactor design may be needed to commercialize economically viable green hydrogen.

Rigorous solar water-splitting technoeconomic analyses have concluded that photoactive particle-based reactors have the potential to generate H_2 at a lower cost than either a PV + electrolyzer or flat-panel photoelectrochemical (PEC) system.⁵⁻⁷ Numerous particulate

photocatalyst systems have been investigated, though few have been capable of unassisted solar water-splitting, and photoconversion efficiencies have generally been quite low.⁸⁻¹³ Semiconductor particle-based reactors face several critical issues which have inhibited their energy-conversion efficiencies and prevented practical commercial deployment.^{8, 14} Key challenges include achieving material stability of the photoactive semiconductor, high recombination and/or poor charge separation of the photogenerated carriers, and the need for wide bandgaps to produce the requisite photovoltage which leads to poor utilization of the solar spectrum.

One approach to achieve high efficiency unassisted solar water-splitting is to use tandem complementary bandgap semiconductors in series to build photovoltage while utilizing more of the solar spectrum. Modeling such tandems has found that an ideal combination of 1.6-1.8 eV and 0.9-1.1 eV bandgaps is capable of > 25% STH efficiency. ^{15, 16} Si, with a bandgap of 1.1 eV, is a prime candidate for the lower subcell of the tandem since it is abundant with an established low-cost production process. Extensive work has shown that Si microwires can be produced cost-effectively with optimal dimensions to match the material quality. ¹⁷⁻¹⁹ With an axial dimension longer than the optical penetration depth ($> 100~\mu m$) and a radius commensurate with the minority-carrier diffusion length (typically $3-10~\mu m$), such microwires can decouple the directions of light absorption and charge-carrier collection and permit the use of cheaper quality Si. ²⁰ Si microwire arrays have been utilized in promising photovoltaic and photoelectrochemical applications. ²¹⁻²³ Si microwires are thus a promising platform for a tandem microparticle structure that could enable high efficiency photochemical reactions.

Several wider bandgap top subcell candidates have been explored in tandem with Si, as both photoanodes and photocathodes. Demonstrated tandem core-shell microstructure combinations

include Si/TiO₂,²⁴ Si/BiVO₄,²⁵ Si/Ga_{1-x}In_xP,²⁶ Si/WO₃,²⁷ Si/Ta₃N₅,²⁸ and Si/CuO₂.²⁹ The microscale dimension of the Si wires in these tandems allows the incorporation of a buried pnhomojunction, which aids charge separation via migration with a built-in electric field. A transparent conductive oxide such as fluorine-doped tin oxide (FTO) is frequently employed as an ohmic contact between the subcell layers.^{24, 27} While materials scientists continue to pursue improved semiconductors to be a top subcell of ideal bandgap which is stable with the necessary photovoltage, the properties of tandem-particle-based photocatalytic reactors can be explored with established materials. In particular, TiO₂, though far from an ideal bandgap top subcell, is a stable photoanode material that provides sufficient photovoltage in combination with Si for unassisted solar water-splitting.^{24, 30}

In our previous work, a proof-of-concept np⁺-Si/FTO/TiO₂ microwire structure capable of unassisted solar hydrogen generation was grown on a Si substrate.³⁰ Detached, free-floating tandem Ni/np⁺-Si/FTO/TiO₂ microparticles were fabricated with a photodeposition process to selectively attach a Ni bulb on the cathodic site of the n-Si core at the wire base. The Ni bulb served as a hydrogen evolution co-catalyst and was demonstrated to enable in-situ magnetic alignment of the suspended tandem microwire slurry.³⁰

An understanding of the parameters which influence the optical properties of a tandem microwire slurry is necessary to improve the corresponding photocatalytic behavior and optimize the efficacy of individual photoactive particles. A high light absorptance with a relatively low volume fraction of photoactive material is an important strategy to improve the cost-effectiveness of the slurry by minimizing particle fabrication expense. Remarkably, a previous study of aligned, substrate-bound Si microwire arrays found that up to 96% light absorption was possible with only 5% areal coverage of Si wires using light management techniques including

scattering particles and a back reflector.³¹ Microwire particles in solution will rapidly settle if unperturbed but can be suspended with uplifting carrier gas bubble flow.³⁰ Unlike nanoscale particle suspensions in which the fluid has fairly homogeneous properties, the microscale dimensions and concentration of the wires and bubbles can lead to complex mesoscale optical phenomena that influence the photochemical performance.^{32, 33}

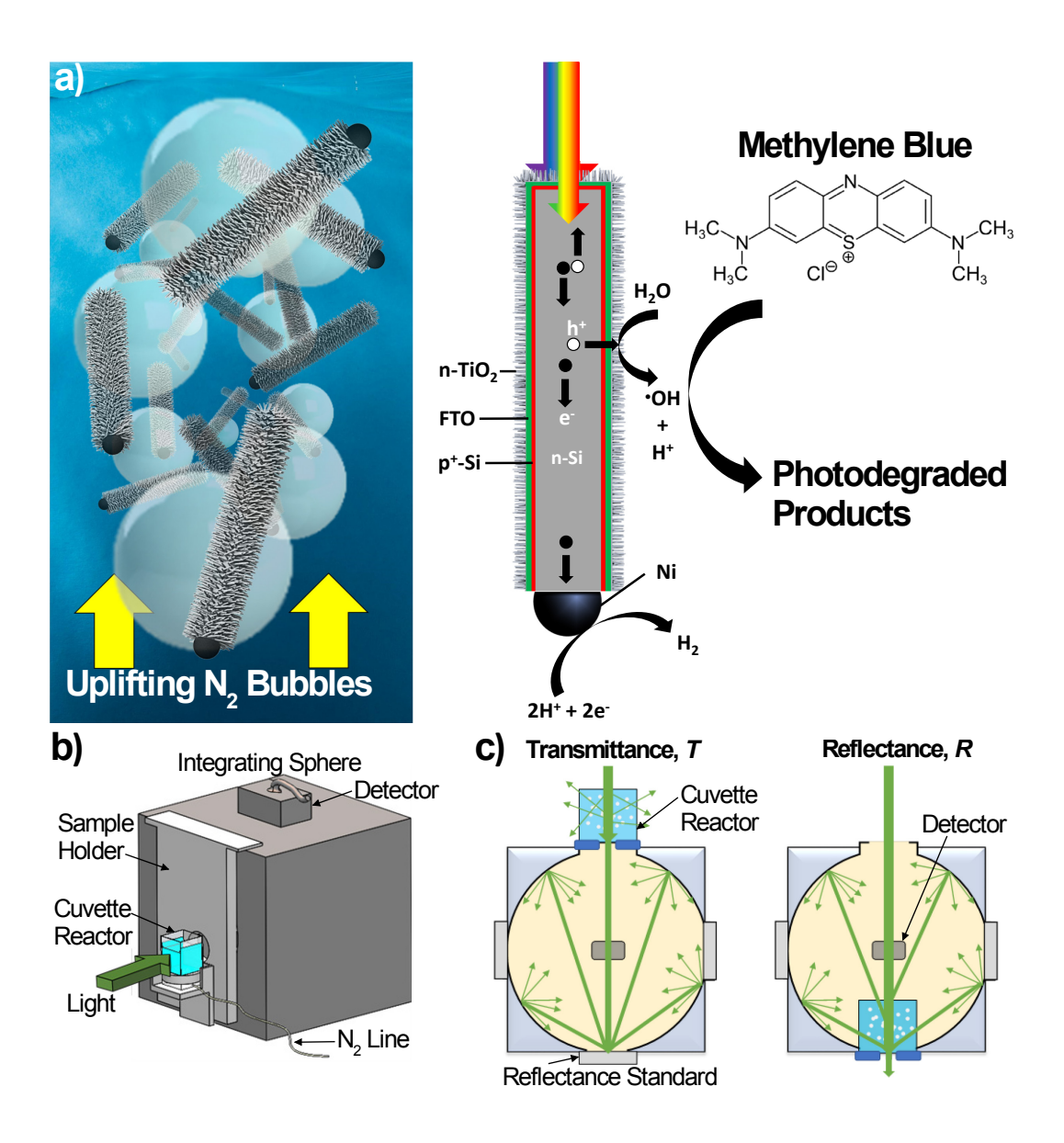


Figure 1. (a) Schematic of a tandem microwire slurry dispersed by uplifting N₂ carrier gas bubbles (left) and the tandem Ni/np⁺-Si/FTO/TiO₂ microstructure driving photodegradation of methylene blue (right). (b) 3D image of the integrating sphere and (c) 2D cross-sectional images

of the modes of operation for measuring transmittance and reflectance with an actively bubbled cuvette reactor.

Herein, the conditions to optimize photoactive microparticle utilization while maintaining an overall high light absorption in the slurry were investigated. The optical properties of the tandem microwires dispersed in aqueous media were characterized to improve the understanding of light propagation through the class of photochemical microparticle slurry reactors. Transmittance and reflectance of the system as a function of wavelength, slurry particle concentration, and dispersion flowrates were measured via UV-Vis spectroscopy with an integrating sphere. Corresponding photochemical performance of the Ni/np⁺-Si/FTO/TiO₂ microwire slurry was characterized via organic methylene blue (MB) dye degradation under visible and UV illumination (Fig. 1). The photodegradation of the MB dye enabled direct in-situ monitoring of the performance under different reactor conditions.

EXPERIMENTAL

Tandem Semiconductor Fabrication

The Ni/np $^+$ -Si/FTO/TiO $_2$ tandem microwire particles were prepared as described in our previous work. 30 Briefly, n-Si microwire arrays (9 µm diameter, 15 µm center-to-center pitch hexagonally close packed) were fabricated using deep reactive ion etching (DRIE) (Washington Nanofabrication Facility). This pattern was then etched into the n-Si wafer by DRIE (SF $_6$ and C4F $_8$, STS Pegasus, SPTS Technologies) to a depth of \sim 100 µm. The microwire array was subsequently cleaned by reactive ion etching with oxygen to remove the residual photoresist.

A B-doped p⁺ radial emitter layer was formed on the n-Si microwire array using diffusion from solid-source BN dopant wafers (Saint Gobain-BN-975) at 950 °C for 4 min under N₂ flow. The silicon wafers were placed between the dopant wafers in a ceramic boat at 950 °C for 4 min under N₂ flow (200 sccm in a 1-inch diameter tube). The boat was slowly removed from the furnace over > 1 min while the temperature ramped down to 750 °C. After cooling, each Si sample was etched in buffered HF for 30 s to remove any unreacted dopant glass and then loaded again at 750 °C under O₂ flow (100 sccm) for 30 min to grow a low temperature oxide (LTO). The cooled wafers were then etched in 10% HF for 1 min to remove any residual Si-B layer oxidized during the LTO step.

A ~500 nm thick FTO, SnO₂:F, layer was spray-deposited on the Si as an ohmic contact layer between the tandem Si and TiO₂ subcell layers. The np⁺-Si planar and/or microwire arrays were again etched with 10% HF for 30 s immediately prior to placing them on a hotplate at 400 °C. FTO was deposited by spraying a fine mist of a precursor solution, which was made by mixing 97% by volume of 0.50 M butyltin trichloride in pure ethanol and 3% by volume of 0.50 M ammonium fluoride in DI water. The FTO layer required 30 cycles of spraying with 3 sprays per cycle with 45 s between cycles to allow the equilibration of the Si sample temperature. The Si samples were rotated after 15 cycles to ensure conformal coverage of the FTO.

A layer of rutile TiO₂ nanorods was subsequently grown on the np⁺-Si/FTO microwire array using a hydrothermal method.³⁴ The Si/FTO samples were placed in 60 mL of an aqueous solution of 0.05 M titanium n-butoxide and 6 M HCl in a Teflon cell. The cell was then put in a hydrothermal autoclave reactor and placed in a muffle furnace at 200 °C for 4 h. The autoclave reactor was then cooled under running water for 15 min. The np⁺-Si/FTO/TiO₂ planar and/or

microwire array samples were then removed from the Teflon cell, rinsed with DI water, and annealed at 450 °C for 30 min in air.

To detach the tandem np⁺-Si/FTO/TiO₂ microwires from the n-Si substrate (projected areas of 0.5 - 1.5 cm²), the back of the wafer was secured to a glass slide with mounting wax, the microwire array was mechanically coated with nail polish polymer, and a razor blade was used to scrape off the microwires embedded in the polymer film.¹⁹ The sacrificial polymer was then dissolved in acetone for > 1 h and the microwires filtered from the solution using a sintered fine glass frit (Chemglass Life Sciences LLC). A photodeposition process was then used to selectively deposit Ni catalyst at the exposed n-Si base of the tandem microwire.³⁰ Ni electroplating solution was added to the DI water containing the detached microwires in a 1:2 volume ratio, and then sodium sulfite (Na₂SO₃, Sigma Aldrich) was dissolved to a concentration of 0.112 M to serve as a hole scavenger. The tandem microwires in the Ni deposition bath were illuminated with AM1.5 light at 1.6 Suns for 3.5 h with added illumination from a UV lamp (3 mW cm⁻², AT1000Ex, Advanced Technologies International) to accelerate the photodeposition of Ni. The wires were then dispersed in 1 mL deionized (DI) water or MB solution for the optical and photocatalytic dye degradation measurements, respectively. The photomask pattern spacing was used to calculate the wafer-area-dependent concentration of particles (see SI). A 1 cm² microwire array wafer area had ~5.13x10⁵ wires.

Optical Characterization

The reflectance, R, and transmittance, T, of the microwire slurry under various conditions of bubble flowrate and particle concentration were measured using UV-Vis spectroscopy with an integrating sphere (Perkin Elmer Lambda 950). A quartz cuvette of 1 cm width x 1 cm depth

cross-section had the base cut off, leaving a 1 cm height, and a microporous glass frit (Chemglass CG-201-09) was sealed to the cuvette using Hysol 9460 epoxy. A cannula tubing inlet was then introduced below the frit and sealed in with the closed bottom base of the quartz cuvette. Custom 3D-printed holders were fabricated for the modified cuvette reactor to fit it to the integrating sphere for reflectance and transmittance mode measurements. The cuvette was filled with 1 mL of particle slurry in DI water and placed on the 3D-printed holder. During operation, N₂ gas was passed through the cannula tubing which pressurized the chamber below the frit and led to microbubble generation which flowed upward and dispersed the microwires in solution. For the transmittance measurement, the cuvette was placed at the integrating sphere entrance port and the exit port was closed by a Spectralon reflectance standard. An air baseline was measured without the cuvette but with the holder on the entrance port. For the reflectance measurement, the cuvette was placed at the integrating sphere exit port such that it was just inside the sphere, while a gap in the holder allowed transmitted light to exit the sphere through the back face of the cuvette. The fraction of light absorbed in the system, the absorptance a, was calculated as a = 1 - R - T for measured reflectance and transmittance values as a function of wavelength.

Photocatalytic Dye Degradation

To measure their photocatalytic activity, the Ni/np⁺-Si/FTO/TiO₂ microwires were dispersed in an aqueous solution of 40 μM MB (VWR International) and 0.01 M Na₂SO₄ which was deaerated with N₂ for 60 min prior to any measurement. In addition, tandem semiconductor samples were pre-soaked in the MB solution for 60 min or more before photocatalytic measurements to reach a steady-state level of dye adsorption on the surface. Two-electrode photoelectrochemical current density vs. potential (*J-E*) behavior in MB solution was measured

under similar conditions using a BioLogic SP-200 potentiostat. The reference, in this case, was shorted to a Ni foil counter electrode immediately adjacent to a planar tandem semiconductor working electrode without a separator. Illuminated experiments were performed under a 1-Sun intensity of 100 mW cm⁻² generated with a 300 W Xenon lamp (Newport 6258) with an AM1.5 global filter (Newport 81094). During spectral mismatch measurements, higher energy photons including the UV were eliminated with a longpass filter (Newport 20CGA-800) with a cutoff for wavelengths less than 800 nm. In some experiments, an external UV-LED lamp (Hamamatsu, L14310-120, light at 365 nm) was used at variable power levels to supply additional UV light bias to generate higher photocurrent in the TiO₂. The optical absorption spectra of the MB solution was measured using a double-beam UV-Vis spectrophotometer (Cary 60 UV-Vis), and MB degradation was monitored by tracking the absorbance value at $\lambda_{max} = 664$ nm and normalizing to the initial absorbance at the beginning of the measurement.

Materials Characterization

Electron micrographs of the morphology and elemental analysis of the microwires were performed with a Thermo Fisher Apreo C LoVac field emission scanning electron microscope (SEM) and energy-dispersive X-ray spectroscopy (EDS) detector.

RESULTS AND DISCUSSION

Tandem Microwire Slurry Optical Properties

Because of the tendency of microparticles and bubbles in the slurry to scatter light, an accurate measurement of the optical properties required the use of an integrating sphere to account for the

diffuse light (Fig. 1). Transmittance and reflectance were measured separately in different operating modes and used to calculate the absorptance in the slurry. UV-Vis spectroscopy employed a broad wavelength range of 200 - 1100 nm to cover photon energies greater than the bandgaps of either the Si or TiO₂ subcell layers. A generalized energy band diagram for the tandem Ni/np⁺-Si/FTO/TiO₂ structure is shown in Fig. S1. The *T*, *R*, and *a* values of the slurry were measured for variable dispersive N₂ bubble flowrates (25 – 35 sccm) and different concentrations of tandem microwires (12.4 – 37.1 g L⁻¹, corresponding to a photoactive volumetric percentage of 0.34 – 1.01%, see SI for the calculation). Lower N₂ flowrates were observed to lead to inactive areas of the bubbling frit and eventual settling of microwires in the solution dead space.

The optical properties of the slurry were measured as a function of bubble flowrate for three microwire concentrations as well as in the absence of photoactive particles (Fig. 2 and Fig. S2). Without tandem microwires, the bubbling DI water exhibited fairly high specular transmittance of $\sim 60 - 70\%$, and a corresponding reflectance of $\sim 20 - 30\%$ (Figs. 2a-b). Increased flowrate led to a slight increase in reflectance and decrease in transmittance due to scattering off the bubbles, but the difference was minimal. The absorbance peak at 970 nm was attributed to light absorption in the DI water (Fig. 2c).

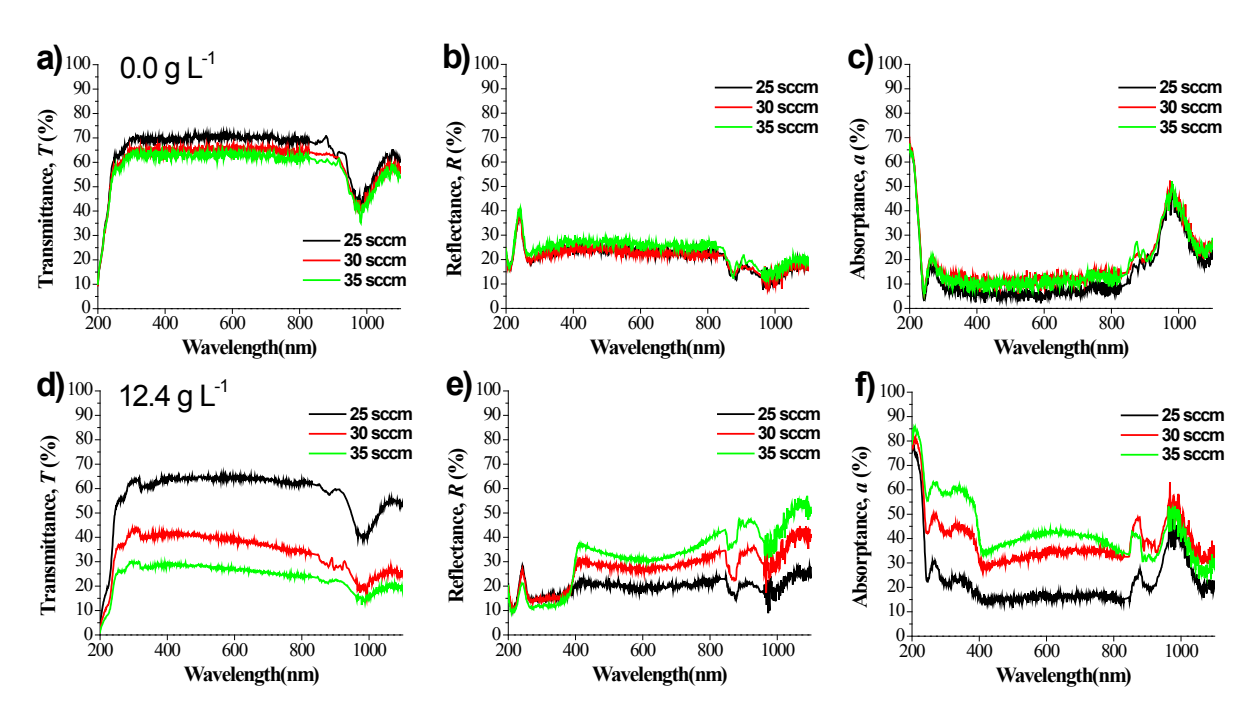


Figure 2. Measured (a, d) transmittance, (b, e) reflectance, and (c, f) absorptance vs. wavelength for different carrier gas N₂ bubble flowrates for tandem microwire concentrations of (a-c) 0.0 and (d-f) 12.4 g L⁻¹.

Upon the addition of tandem microwires to the DI water, the flowrate dependence of the optical properties became more pronounced. At the lowest particle concentration tested, 12.4 g L^{-1} , transmittance at visible wavelengths was $\sim 60\%$ at 25 sccm (Fig. 2d), only slightly lower than the case without particles. However, increasing the N₂ flow to 35 sccm decreased T to $\sim 25\%$, which demonstrates the importance of a robust bubble flow to keep the microwires well dispersed and thus highly absorbing as a slurry. Although the effect on reflectance was less notable, the bubble flowrate was a significant factor in minimizing the transmittance for all three tandem microwire concentrations tested. Consequently, the absorptance increased with bubble flowrate as well. Optical data for the other slurry microwire concentrations are shown in Fig. S2.

The tandem particles were observed to be uniformly dispersed under vigorous bubbling at 35 sccm, and thus this condition was selected as the default flowrate for future experiments. Figure 3 shows the optical properties of slurries as a function of tandem microwire concentration and corresponding photoactive volume percentage. The visible region transmittance decreased from a value of \sim 60% without microwires to \sim 25% with 12.4 g L⁻¹ to as low as \sim 5% with 37.1 g L⁻¹ of tandem particles. Notably, this dramatic drop in T was accomplished with only 1% of the slurry volume filled with photoactive particles. Although there was a slight increase in R at wavelengths > 400 nm in the presence of tandem microwires, most of the decreased transmittance was attributable to an increase in the slurry absorptance at higher particle concentrations, reaching as high as 87% at 300 nm (Fig. 3c). This particle concentration of 37.1 g L⁻¹, from harvesting the tandem microwires from a 1.5 cm² array, was used as the default condition for subsequent photochemical experiments.

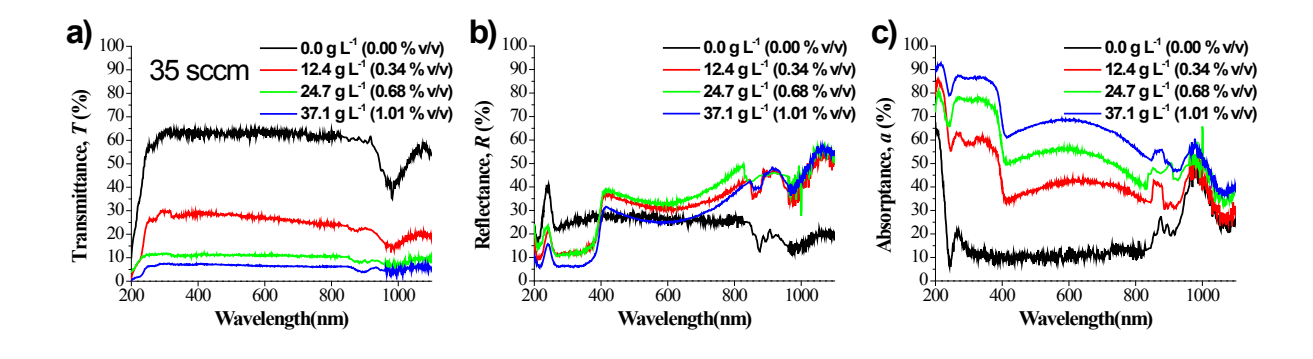


Figure 3. Measured (a) transmittance, (b) reflectance, and (c) absorptance vs. wavelength for different tandem microwire concentrations (and corresponding volume percentage) for slurries at a bubble flowrate of 35 sccm.

The shape of the absorptance curves is indicative of the tandem microstructure in DI water. The spectra showed a sharply increasing absorptance at wavelengths < 400 nm. This transition

marks the onset of photon energies capable of exciting electrons across the TiO₂ bandgap. Any photons at this energy not absorbed in the TiO₂ layer can still be absorbed in the underlying Si microwire core, and thus absorptance in this region is higher than the wavelengths that can only be absorbed by Si. Between 400 – 900 nm, light absorption was primarily due to the Si and peaked at ~70% at 600 nm for 37.1 g L⁻¹ (Fig. 3c). Decreasing absorptance at longer wavelengths is consistent with the indirect bandgap of Si and corresponding drop in the absorption coefficient for photon energies closer to the 1.1 eV bandgap. This effect would be exacerbated for light incident on horizontally oriented microwires, resulting in absorption through the much shorter radial dimension as opposed to the longer axial dimension. The absorptance peak at 970 nm was due to water absorption in the infrared (Fig. 2c), and the uneven shift at 850 – 900 nm was attributed to signal noise during an automated UV-Vis detector switch.

Photocatalytic Performance via Methylene Blue Degradation

Because of the in-situ photocatalytic characterization advantages of using an indicator dye and the difficulty of accurately quantifying H₂/O₂ in the presence of the slurry carrier gas flow, methylene blue degradation was the primary method utilized to characterize slurry photochemical performance. MB, an organic dye, is a model compound for testing the performance of the tandem particles because it provides a simple and standard way of measuring photocatalytic activity in liquid-phase reactions.³⁵⁻³⁹ The MB photodegradation behavior with time was examined under variable conditions of tandem Ni/np⁺-Si/FTO/TiO₂ microparticle concentration, dispersive N₂ bubble flowrate, illumination spectral conditions and UV intensity, and light management techniques including highly-reflective alumina particles or a back reflector.

The general mechanistic pathway for the degradation of the MB dye has been reported to proceed through free radical species. Photogenerated charge-carriers lead to the formation of *O₂ and *OH radicals which subsequently attack the aromatic rings of the MB molecule to break it down into intermediates and eventually into CO₂ and H₂O.⁴⁰ The MB degradation is readily monitored by tracking the decay in the main absorbance peak via UV-Vis spectroscopy (Fig. S3). The ${}^{\bullet}O_2^{-}$ radical, however, is formed from photoexcited electrons reducing O_2 . ${}^{39, 40}$ Under ongoing N₂ carrier gas bubble flow, the MB solution herein becomes depleted of dissolved O₂, slowing this radical pathway. To prevent the presence of variable concentrations of dissolved O2 from convoluting the results, the MB solution was thoroughly deaerated with N2 for an hour prior to measurements for consistency. MB degradation was thus assumed to proceed primarily through the oxidative formation of *OH radicals, which leads to slower rates of absorbance decay than can be observed in the presence of dissolved oxygen as shown in Fig. S4. It is also known that some MB dye can adsorb onto surfaces, leading to a drop in absorbance that is not attributable to photocatalytic activity.³⁹ To minimize adsorption effects during experiments, photoactive samples were pre-soaked in the MB solution during the 1-hour deaeration to allow adsorption to equilibrate on the frit and tandem samples prior to illumination.

Effect of planar vs. microwire slurry form factor. The first MB photodegradation experiments compared the performance of a tandem microwire slurry to that achievable with a planar tandem device. Planar tandem samples can be electrically connected to make an np⁺-Si/FTO/TiO₂ photoanode to directly measure the current density vs. potential (*J-E*) energy-conversion performance. Two-electrode *J-E* curves under 1 Sun AM1.5 of a planar tandem vs. Ni in 1 M KOH and in the MB solution are shown in Fig. S5. The structure is capable of unassisted solar water-splitting, but the *J-E* curve fill factor and onset potential was worse in the MB solution due

to the low concentrations and relatively high ohmic resistance. Figure 4 shows the normalized absorbance, A/A₀, of MB over the course of an hour under illumination for a planar tandem compared to a tandem microwire slurry. A blank MB solution did exhibit a slight drop in absorbance when illuminated, indicating that a slow direct photoexcited deactivation of the dye occurs as well. In all cases throughout the study, however, the presence of photoactive samples accelerated the rate of decreasing absorbance, consistent with photocatalysis of the MB degradation. The response of the illuminated blank MB solution was compared to an illuminated solution containing only photo-inactive alumina scattering particles to demonstrate that the increased MB photodegradation measured in the presence of tandem microwire slurries could not be attributed solely to an increased optical path length from scattering (Fig. S6).

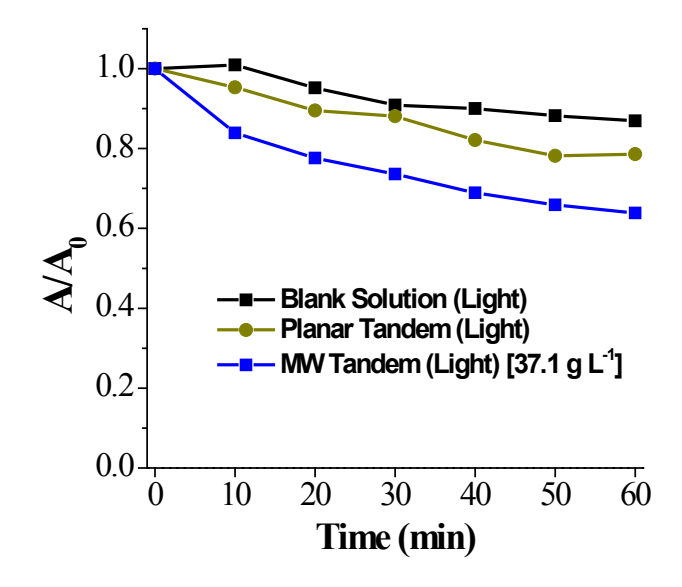


Figure 4. Normalized absorbance of MB vs. time for the blank solution and tandem Ni/np⁺-Si/FTO/TiO₂ planar and microwire slurry samples under 1 Sun AM1.5 illumination at a dispersive bubble flowrate of 35 sccm.

While the planar tandem showed increased decay of the absorbance relative to the blank, the tandem microwire slurry exhibited faster MB photodegradation. Better performance from the microwire slurry compared to the planar form factor was somewhat surprising considering that planar electrodes routinely outperform microwire array electrodes in photoelectrochemical studies. ^{22, 24, 30, 41} Lower planar performance could be partially attributed to a smaller sample area (necessary to fit it in the cuvette reactor) compared to the wafer area used to harvest the microwires, but the volumetric photoactive tandem component was comparable. We speculate that ohmic overpotential, which is significant in the MB solution (Fig. S5), inhibits the planar sample to a greater degree than the microwires. ⁴² Ion conduction between the anodic TiO₂ and cathodic Ni sites must follow a much longer pathway on a macroscopic planar sample compared to the corresponding microscopic distance on a microwire.

Tandem microwires were also analyzed for morphological and chemical changes from photochemical operation as a slurry. Figures 5 and S7 show SEM images of individual microwires before and after a MB photodegradation measurement. For the large majority of observed microwires, there was no indication of dissolution or breakdown of the TiO2 or Si components. In a few cases, regions of the TiO2 nanowire coating shell appeared physically damaged, presumably from aggressive collisions during vigorous dispersal (Fig. S8). After operation, some microwires had lost their Ni bulb (Fig. 5), indicating that co-catalyst adhesion may need improvement (e.g., via sintering) for increased photochemical durability. However, most of the slurry was still attracted to a rare-earth magnet, suggesting intact Ni structures for most wires. Otherwise, EDS analysis indicated no other notable changes in the elemental composition of the structure (Fig. S9). Reuse of the same set of tandem microwires for a subsequent MB photodegradation measurement under the same operating conditions led to a

modest decrease in photocatalytic activity, in which additional surface adsorption of dye and loss of some microwires during additional filtration steps may have contributed to a slurry performance decrease due to any microwire instabilities. (Fig. S10).

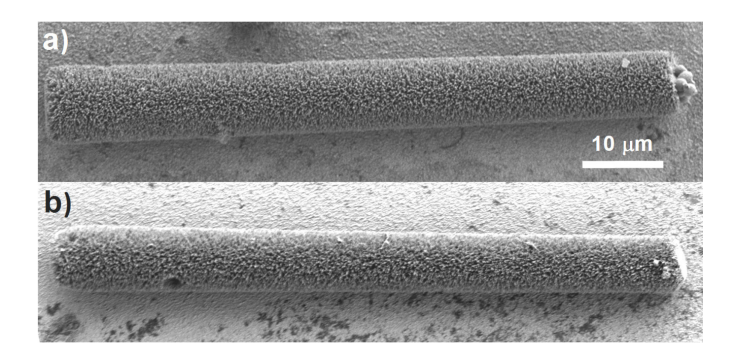


Figure 5. SEM images of tandem microwires (a) before and (b) after a 1-hour MB photodegradation experiment. Scale bar is 10 μm for both images.

Effect of tandem particle concentration. The effect of the tandem microwire concentration on the slurry photochemical activity was investigated with concentrations of 12.4, 24.7, and 37.1 g L⁻¹, corresponding to photoactive volume percentages of 0.34, 0.68, and 1.01 % v/v, derived from harvesting the microwires from 0.5, 1.0, and 1.5 cm² growth substrates, respectively. Figure 6 shows the resulting MB degradation with time at a dispersive bubble flowrate of 35 sccm. In the dark, the absorbance remained relatively steady even for the highest concentration of tandem microwires, indicating that dye adsorption was not a significant source of absorbance loss after the initial pre-experiment equilibration period. Again, in the absence of photoactive particles, a blank MB solution still displayed some non-negligible absorbance decay under 1 Sun AM1.5 illumination. Methylene blue absorbs light most strongly in the 500 – 700 nm region (Fig. S3) and undergoes self-decomposition via electronic transition and intersystem crossing.⁴⁰ The kinetics of MB degradation are complex, with several intermediate reactions and peroxide

formation possible.³⁹ Quantitatively correlating the measured absorptance values (Fig. 3c) to the rate of MB absorbance decay is therefore difficult. However, a higher absorptance leads to an increased rate of charge-carrier photogeneration, a concomitant increase in radical species formation and subsequent dye degradation, and thus a faster decrease in the MB solution absorbance. This qualitative trend held for the photoactive slurries, with higher tandem microwire concentrations leading to greater absorbance decay (Fig. 6).

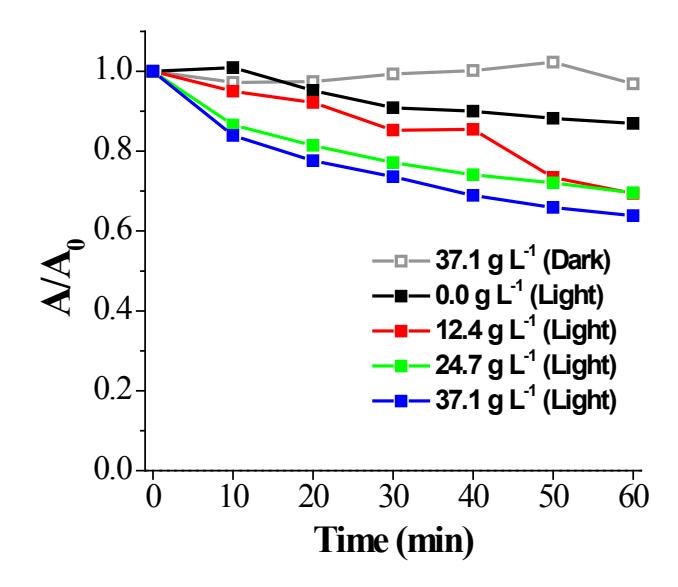


Figure 6. Normalized absorbance of MB vs. time for the blank solution and tandem microwire slurries of varying particle concentration in the dark or under 1 Sun AM1.5 illumination at a dispersive bubble flowrate of 35 sccm.

Effect of carrier gas dispersive bubble flowrate. MB photodegradation was characterized vs. N₂ flowrate (25 – 35 sccm) for the 37.1 g L⁻¹ particle concentration which had yielded peak absorptance (Fig. 3c). The resulting normalized MB absorbance vs. time with varying flowrate is shown in Figure 7. Although increased bubble flowrate did lead to greater MB degradation, the difference from 25 to 35 sccm was minor (at most 5.4% lower for 35 sccm at 20 min). Notably, a

slurry of this microwire concentration also did not vary greatly in its optical properties within this range of flowrates (Fig. S2d-f). The reflectance showed almost no change with flowrate, while the absorptance displayed less variation than at lower particle concentrations (Fig. S2e-f). The limited dependence of MB photodegradation on flowrate within the 25 – 35 sccm range was thus consistent with the light management within the slurry as measured with the integrating sphere. No performance improvement was observed at higher flowrates either. The main role of the bubbles was to uniformly suspend the microwires, and at 25 sccm and above for this particle concentration there was no significant change from bubble light scattering. However, as previously mentioned, below 25 sccm bubbling from the frit became uneven and dead spots in the microwire fluidization were observed. A MB photodegradation experiment at 20 sccm was performed to highlight the consequences of non-uniform particle dispersion. As the flowrate dropped below the critical threshold for producing bubbles evenly across the frit, the tandem microwires were poorly suspended in these regions which resulted in locally decreased particle concentration. Consequently, the MB absorbance remained appreciably higher at 20 sccm than the other measured flowrates, in accordance with the microwire-concentration-dependent slurry photochemical behavior (Fig. 6).

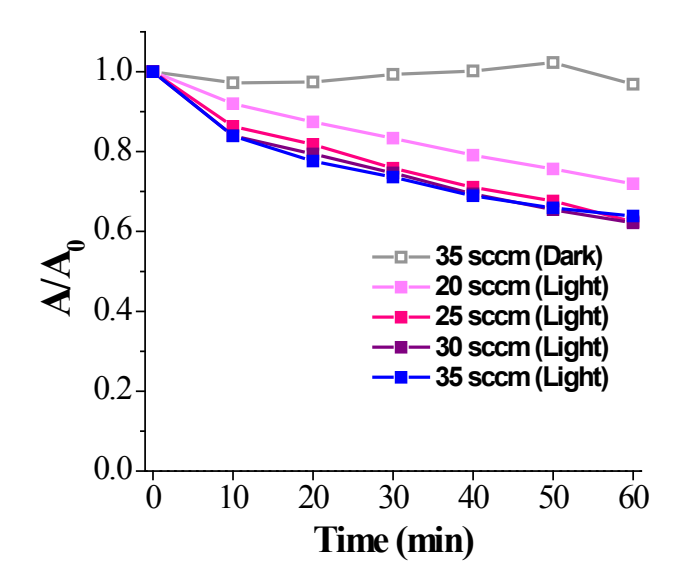


Figure 7. Normalized absorbance of MB vs. time for tandem microwire slurry samples of 37.1 g L⁻¹ particle concentration in the dark or under 1 Sun AM1.5 illumination at varying dispersive bubble flowrates.

Effect of spectral mismatch. The TiO₂ and Si tandem combination is capable of generating sufficient photovoltage for unassisted solar water-splitting by connecting the subcell layers in electrical series. However, like all series-connected tandems, the current flowing through each subcell unit of the circuit must be matched. If one semiconductor layer underperforms the other in photocurrent, the partner subcell current will be limited, thus more strongly decreasing the efficiency of the overall tandem device. Spectral mismatch is one way in which tandem devices are detrimentally affected by their current-matching requirement, in which the spectral distribution of the illumination deviates from the standard AM1.5 and changes the relative above-bandgap photon flux to each subcell layer. Although the Ni/np⁺-Si/FTO/TiO₂ tandem structure is not an ideal bandgap combination for balanced photocurrents at AM1.5, it is still

illustrative to investigate the slurry photochemical performance as the photon flux to each photoactive semiconductor layer is varied.

Illumination sources targeting the narrow bandgap Si and wider bandgap TiO₂ were provided with longpass-filtered AM1.5 and a UV LED, respectively. Using a filter to eliminate the AM1.5 wavelengths below 800 nm (i.e., the UV and parts of the visible spectrum), the activity of the tandem microwire slurry for MB photodegradation was dramatically decreased compared to the full unfiltered 1 Sun AM1.5 (Fig. 8). The 800 nm cutoff wavelength was chosen to avoid the main absorbance peak of MB at ~660 nm (Fig. S3), to ensure that the filtered light was only exciting the Si microwire core. TiO₂ is the current-limiting subcell layer under unfiltered AM1.5 (Fig. S5), but after applying the longpass filter there are almost no photons capable of exciting electrons across its bandgap. Consequently, the TiO₂ photocurrent plummeted under longpass-filtered light, series-limiting the tandem microwires and causing the MB photodegradation activity to drop sharply.

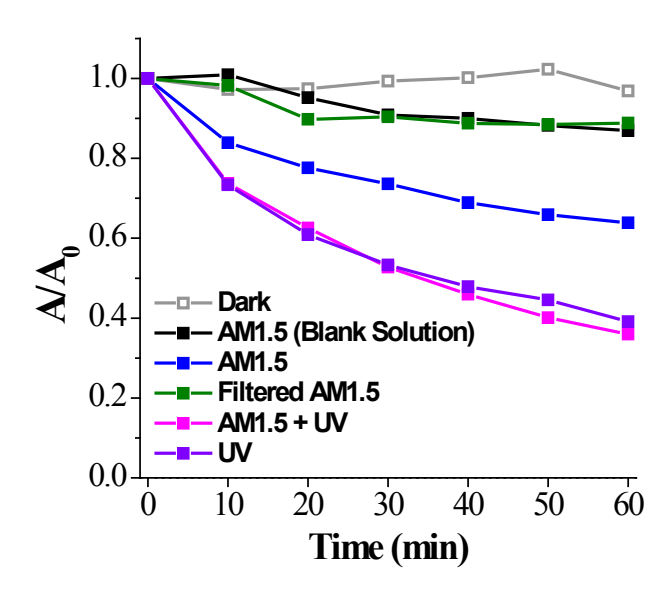


Figure 8. Normalized absorbance of MB vs. time for tandem microwire slurries under different light conditions. AM1.5 illumination was 1 Sun and unfiltered unless labeled otherwise. Filtered AM1.5 used a longpass filter to cut off wavelengths less than 800 nm. UV excitation was 60 mW cm⁻² at 365 nm. Except for the blank solution, all slurries had a particle concentration of 37.1 g L⁻¹. The N₂ flowrate was 35 sccm.

On the other hand, the addition of an extra UV optical bias to the AM1.5 illumination led to significantly higher MB photodegradation. As the outer shell of the core-shell tandem microwire structure, the TiO₂ gets the first opportunity to absorb the above-bandgap monochromatic light produced by the UV LED at 365 nm. Because the wide bandgap of TiO₂ is current-limiting to the Si subcell under AM1.5, moderate increases to the TiO₂ photocurrent can be sustained by the full tandem, leading to proportionately enhanced photochemical activity.

When illuminating with just the UV source, one might naively predict decreased performance for the tandem microwire slurry due to subcell current-matching limitations comparable to the performance under longpass-filtered AM1.5. A rutile TiO₂ layer of comparable thickness to the microwire shell (~1.5 μm) can be calculated by the Beer-Lambert law to transmit much less than 1% of the photons at 365 nm,⁴³ thus leading to a condition severely current-limited by the inadequate availability of light for the underlying Si subcell. However, the tandem microwire slurry under the UV source alone displayed comparable MB photodegradation activity to the AM1.5 + UV condition (Fig. 8). In this case, the morphology of the TiO₂ shell layer may partially explain the lack of a spectral mismatch current-limited response in the tandem microwire. Rather than a compact, contiguous layer, the hydrothermal rutile TiO₂ synthesis produces a coating of TiO₂ nanorods (Fig. 5) that may enable a portion of the incident illumination to pass between nanorods and across the FTO layer to excite the Si core.^{30, 34} Thus, the UV source could excite both subcell layers to enable the tandem microwire to have high MB

photodegradation activity despite the presumed spectral mismatch. Photoelectrochemical *J-E* behavior of a planar tandem under only the UV excitation showed that the photocurrent was decreased but not as severely as would be expected if the Si subcell had little to no photogeneration (Fig. S5). We speculate the strong tandem performance under only UV may also be attributable to highly excited UV-generated holes in the TiO₂ valence band leading to radical species formation and degradation of adsorbed and near-surface MB faster than tandem current-limitations can force recombination.

Effect of UV light bias. As mentioned, the wide bandgap of TiO₂ is not an ideal match to Si for a current-matched tandem under AM1.5 illumination. Consequently, the TiO₂ photocurrent was limiting for the Ni/np⁺-Si/FTO/TiO₂ tandem device. TiO₂ was used in the present system for its large photovoltage and photoanodic durability for water-splitting. An ideal replacement top subcell layer would generate a higher photocurrent from a narrower bandgap while still providing the requisite photovoltage for water-splitting in combination with Si. Improved performance for a tandem not as limited by the top subcell photocurrent can be simulated by adding an optical light bias of a wavelength sufficient to excite the wider bandgap. Improved tandem microwire slurry photochemical performance was demonstrated with a UV optical bias at several intensities (Fig. 9). As expected, higher intensity optical bias led to greater MB photodegradation. A significant enhancement in the rate of MB absorbance decay was observed upon adding UV bias, but further increases of x2 and x3 in the UV intensity led to only modestly faster MB photodegradation.

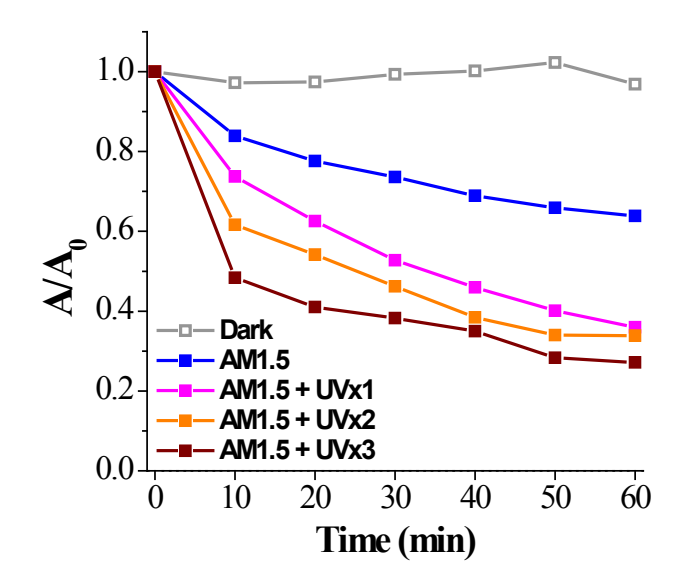


Figure 9. Normalized absorbance of MB vs. time for tandem microwire slurries under illumination with increasing UV optical bias, from 1 Sun AM1.5 alone and then with added UV excitation ($x1 = 60 \text{ mW cm}^{-2}$, $x2 = 120 \text{ mW cm}^{-2}$, $x3 = 180 \text{ mW cm}^{-2}$). All slurries had a particle concentration of 37.1 g L⁻¹. The N₂ flowrate was 35 sccm.

Effect of scattering particles and back reflection. Light management techniques are a potentially useful strategy to increase the photochemical conversion efficiency of the slurry without unnecessarily driving up costs with excessively high photoactive tandem microwire concentrations. Previously, vertically aligned Si microwire arrays constituting only 5% of the projected area were modified to enable 96% light absorptance independent of the angle of incidence. In that study, light was redirected and concentrated in the Si by introducing Al₂O₃ particles within the microwire array to scatter photons passing between microwires, and a back-reflector layer behind the microwire array redirected light for a second opportunity at absorption. Similar light management strategies were investigated in this work to concentrate light in the photoactive microwires.

Alumina particles of ~5 µm diameter were mixed at two different concentrations with the tandem Ni/np⁺-Si/FTO/TiO₂ microwire slurry. Figure 10 shows the resulting MB photodegradation behavior in comparison to the microwire slurry without scattering particles. Unlike the case of alumina scattering particles within a vertically aligned microwire array,³¹ scattering particles mixed within a three-dimensionally dispersed microwire slurry proved to be detrimental to the photoactive performance. At only 3.0 g L⁻¹, Al₂O₃ particles slightly decreased the MB photodegradation, while an increase of the concentration to 6.0 g L⁻¹ led to a severe decline in the absorbance decay. Notably, in the case of the reported aligned microwire array, the alumina scattering particles were confined to a region between Si microwires so that any light scattered by the alumina had a high likelihood of being reflected into the photoactive material.³¹ In the slurry medium, however, the photoactive microwires and alumina particles were intermixed and free to disperse within the solution volume. As such, light entering the cuvette from one side can encounter alumina particles which scatter light back out of the reactor before it has the opportunity to be absorbed by photoactive microwires deeper in the slurry. A higher concentration of alumina particles thus had the effect of reflecting more light out of the cuvette, as shown in example integrating sphere measurements in Fig. S11. An increasing concentration of alumina particles thus decreased the absorptance of the slurry, making intermixed reflective scattering particles an ineffective light management technique for photoactive particle suspension reactors.

On the other hand, the inclusion of a BaSO₄ reflective layer at the back and sides of the cuvette reactor led to a notable improvement in the MB photodegradation activity of a tandem microwire slurry (Fig. 10). Barium sulfate has high diffuse reflectance and is the same material used to coat the interior of the integrating sphere. Thus, BaSO₄ made an ideal Lambertian back reflector to

redirect transmitted light back into the slurry for another chance to be absorbed. After 1 hour of illumination with a back reflector, the tandem microwire slurry decreased the MB normalized absorbance another 10% beyond what it achieved in the absence of back reflection. Thus, back reflectors could be a critical tool for optimizing performance and mitigating costs in microparticle suspension reactors.

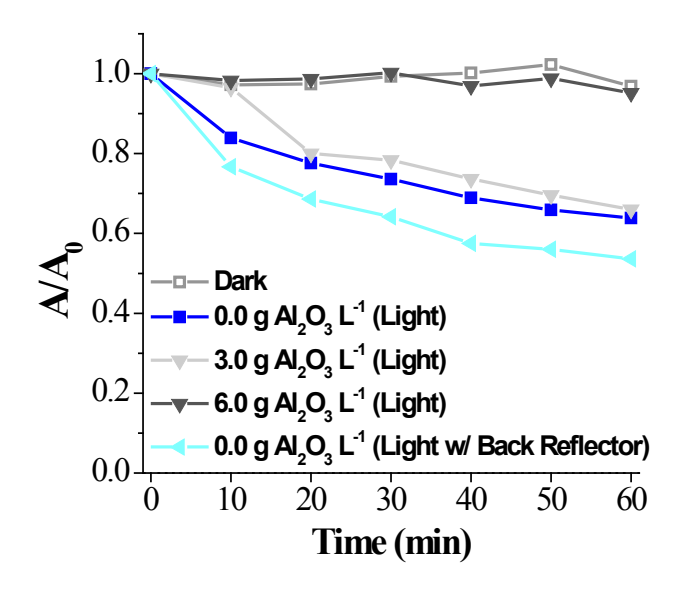


Figure 10. Normalized absorbance of MB vs. time for tandem microwire slurry samples with added Al₂O₃ light scattering particles at a concentration of 0.0, 3.0, or 6.0 g L⁻¹ and one case with a BaSO₄ back reflector. All slurries had a tandem microwire particle concentration of 37.1 g L⁻¹. The N₂ flowrate was 35 sccm. Illumination was 1 Sun AM1.5.

CONCLUSIONS

Tandem semiconductor structures provide a pathway to achieving high water-splitting STH efficiency, and particle suspension reactors may be the lowest cost option for solar hydrogen generation. The proof-of-concept Ni/np⁺-Si/FTO/TiO₂ microwires used herein are capable of unassisted solar water-splitting and were used as a platform to investigate the optical properties

of tandem microparticle slurries while methylene blue indicator dye was used for the in-situ monitoring of photochemical activity. The dispersive carrier gas bubbles had little effect on the photoactivity above a threshold flowrate, but below this flowrate, insufficient bubbling led to ineffective and non-uniform particle suspension and decreased absorbance and photoactivity. Higher photoactive particle concentrations enabled faster MB photodegradation, but notably, a 1% volumetric concentration of tandem microwires was sufficient for 70 – 85% light absorption. Absorptance and corresponding MB photodegradation was even higher when employing a back reflector layer, although photo-inactive light scattering particles actually increased the reflectance loss of the overall slurry. By understanding mesoscale phenomena and light management in a complex medium of bubbles and tandem microwires, operational conditions can be selected to maximize absorbance within each photoactive particle. These optical trends can be extrapolated to other tandem semiconductor particulate systems to lower materials costs and help the field work towards practical, economical solar hydrogen generation.

ASSOCIATED CONTENT

Supporting Information.

The following files are available free of charge.

Tandem microwire density and volume fraction calculations; tandem Ni/np⁺-Si/FTO/TiO₂ structure band diagram; additional tandem microwire slurry optical properties; UV-Vis spectroscopy absorbance spectrum for the methylene blue solution; effect of dissolved oxygen on methylene blue photodegradation; photoelectrochemical energy-conversion behavior; methylene blue photodegradation control experiments; tandem microwire materials characterization;

tandem microwire slurry reuse for methylene blue degradation; slurry optical properties with

alumina scattering particles (PDF)

AUTHOR INFORMATION

Corresponding Author

* E-mail: joshua.spurgeon@louisville.edu, Phone: 502-852-4520

Author Contributions

The manuscript was written through contributions of all authors. All authors have given approval

to the final version of the manuscript. S.G. developed methodology, conducted most of the

experimental investigation, and did the original draft writing. M.C.M. performed the SEM/EDS

investigation. T.C.T. developed the UV-Vis integrating sphere methodology. J.M.S. was

responsible for conceptualization, supervision, project administration, funding acquisition, and

review and editing of the writing.

Funding Sources

United States National Science Foundation under Grant No. 1943977.

ACKNOWLEDGMENT

The authors acknowledge support from the Conn Center for Renewable Energy Research at the

University of Louisville. This material is based upon work supported by the United States

National Science Foundation under Grant No. 1943977. We would also like to thank Dr. Gautam

Gupta for the use of his UV-Vis spectroscopy system.

29

REFERENCES

- 1. Jia, J. Y.; Seitz, L. C.; Benck, J. D.; Huo, Y. J.; Chen, Y. S.; Ng, J. W. D.; Bilir, T.; Harris, J. S.; Jaramillo, T. F., Solar water splitting by photovoltaic-electrolysis with a solar-to-hydrogen efficiency over 30%. *Nat. Commun.* **2016**, *7*, 13237, DOI 10.1038/ncomms13237.
- 2. Licht, S.; Wang, B.; Mukerji, S.; Soga, T.; Umeno, M.; Tributsch, H., Efficient solar water splitting, exemplified by RuO₂-catalyzed AlGaAs/Si photoelectrolysis. *J. Phys. Chem. B* **2000,** *104*, 8920-8924, DOI 10.1021/jp002083b.
- 3. Luo, J. S.; Im, J. H.; Mayer, M. T.; Schreier, M.; Nazeeruddin, M. K.; Park, N. G.; Tilley, S. D.; Fan, H. J.; Gratzel, M., Water photolysis at 12.3% efficiency via perovskite photovoltaics and Earth-abundant catalysts. *Science* **2014**, *345*, 1593-1596, DOI 10.1126/science.1258307.
- 4. Nima Simon, M. M., Heidi Larson, P.E. Examining the current and future economics of hydrogen energy. https://www.icf.com/insights/energy/economics-hydrogen-energy.
- 5. Shaner, M. R.; Atwater, H. A.; Lewis, N. S.; McFarland, E. W., A comparative technoeconomic analysis of renewable hydrogen production using solar energy. *Energy Environ. Sci.* **2016**, *9*, 2354-2371, DOI 10.1039/c5ee02573g.
- 6. James, B. D.; Baum, G. N.; Perez, J.; Baum, K. N., Technoeconomic Analysis of Photoelectrochemical (PEC) Hydrogen Production. *US Department of Energy* **2009**, DOI.
- 7. Pinaud, B. A.; Benck, J. D.; Seitz, L. C.; Forman, A. J.; Chen, Z. B.; Deutsch, T. G.; James, B. D.; Baum, K. N.; Baum, G. N.; Ardo, S.; Wang, H. L.; Miller, E.; Jaramillo, T. F., Technical and economic feasibility of centralized facilities for solar hydrogen production via photocatalysis and photoelectrochemistry. *Energy Environ. Sci.* **2013**, *6*, 1983-2002, DOI 10.1039/c3ee40831k.

- 8. Fabian, D. M.; Hu, S.; Singh, N.; Houle, F. A.; Hisatomi, T.; Domen, K.; Osterlohf, F. E.; Ardo, S., Particle suspension reactors and materials for solar-driven water splitting. *Energy Environ. Sci.* **2015**, *8*, 2825-2850, DOI 10.1039/c5ee01434d.
- 9. Goto, Y.; Hisatomi, T.; Wang, Q.; Higashi, T.; Ishikiriyama, K.; Maeda, T.; Sakata, Y.; Okunaka, S.; Tokudome, H.; Katayama, M.; Akiyama, S.; Nishiyama, H.; Inoue, Y.; Takewaki, T.; Setoyama, T.; Minegishi, T.; Takata, T.; Yamada, T.; Domen, K., A Particulate Photocatalyst Water-Splitting Panel for Large-Scale Solar Hydrogen Generation. *Joule* **2018**, *2*, 509-520, DOI 10.1016/j.joule.2017.12.009.
- 10. Wang, Q.; Hisatomi, T.; Jia, Q. X.; Tokudome, H.; Zhong, M.; Wang, C. Z.; Pan, Z. H.; Takata, T.; Nakabayashi, M.; Shibata, N.; Li, Y. B.; Sharp, I. D.; Kudo, A.; Yamada, T.; Domen, K., Scalable water splitting on particulate photocatalyst sheets with a solar-to-hydrogen energy conversion efficiency exceeding 1%. *Nature Materials* **2016**, *15*, 611, DOI 10.1038/nmat4589.
- 11. Wang, Z.; Inoue, Y.; Hisatomi, T.; Ishikawa, R.; Wang, Q.; Takata, T.; Chen, S. S.; Shibata, N.; Ikuhara, Y.; Domen, K., Overall water splitting by Ta₃N₅ nanorod single crystals grown on the edges of KTaO₃ particles. *Nature Catalysis* **2018**, *1*, 756-763, DOI 10.1038/s41929-018-0134-1.
- 12. Wang, Z.; Luo, Y.; Hisatomi, T.; Vequizo, J. J. M.; Suzuki, S.; Chen, S. S.; Nakabayashi, M.; Lin, L. H.; Pan, Z. H.; Kariya, N.; Yamakata, A.; Shibata, N.; Takata, T.; Teshima, K.; Domen, K., Sequential cocatalyst decoration on BaTaO₂N towards highly-active Z-scheme water splitting. *Nat. Commun.* **2021**, *12*, 1005, DOI 10.1038/s41467-021-21284-3.
- 13. Liao, L. B.; Zhang, Q. H.; Su, Z. H.; Zhao, Z. Z.; Wang, Y. N.; Li, Y.; Lu, X. X.; Wei, D. G.; Feng, G. Y.; Yu, Q. K.; Cai, X. J.; Zhao, J. M.; Ren, Z. F.; Fang, H.; Robles-Hernandez, F.;

- Baldelli, S.; Bao, J. M., Efficient solar water-splitting using a nanocrystalline CoO photocatalyst. *Nature Nanotechnology* **2014**, *9*, 69-73, DOI 10.1038/nnano.2013.272.
- 14. Nandy, S.; Savant, S. A.; Haussener, S., Prospects and challenges in designing photocatalytic particle suspension reactors for solar fuel processing. *Chem. Sci.* **2021,** *12*, 9866-9884, DOI 10.1039/d1sc01504d.
- 15. Hu, S.; Xiang, C. X.; Haussener, S.; Berger, A. D.; Lewis, N. S., An analysis of the optimal band gaps of light absorbers in integrated tandem photoelectrochemical water-splitting systems. *Energy Environ. Sci.* **2013**, *6*, 2984-2993, DOI 10.1039/c3ee40453f.
- 16. Gaudy, Y. K.; Gacevic, Z.; Haussener, S., Theoretical maximum photogeneration efficiency and performance characterization of In_xGa_{1-x}N/Si tandem water-splitting photoelectrodes. *APL Materials* **2020**, *8*, DOI 10.1063/5.0007034.
- 17. Kayes, B. M.; Filler, M. A.; Putnam, M. C.; Kelzenberg, M. D.; Lewis, N. S.; Atwater, H. A., Growth of vertically aligned Si wire arrays over large areas (> 1 cm²) with Au and Cu catalysts. *Appl. Phys. Lett.* **2007**, *91*, 103110, DOI 103110

Artn 103110.

- 18. Spurgeon, J. M.; Plass, K. E.; Kayes, B. M.; Brunschwig, B. S.; Atwater, H. A.; Lewis, N. S., Repeated epitaxial growth and transfer of arrays of patterned, vertically aligned, crystalline Si wires from a single Si(111) substrate. *Appl. Phys. Lett.* **2008**, *93*, 032112, DOI 032112 10.1063/1.2959184.
- 19. Plass, K. E.; Filler, M. A.; Spurgeon, J. M.; Kayes, B. M.; Maldonado, S.; Brunschwig, B. S.; Atwater, H. A.; Lewis, N. S., Flexible polymer-embedded Si wire arrays. *Adv. Mater.*2009, 21, 325-328, DOI 10.1002/adma.200802006.

- 20. Kayes, B. M.; Atwater, H. A.; Lewis, N. S., Comparison of the device physics principles of planar and radial p-n junction nanorod solar cells. *J. Appl. Phys.* **2005**, *97*, 114302, DOI 10.1063/1.1901835.
- 21. Putnam, M. C.; Boettcher, S. W.; Kelzenberg, M. D.; Turner-Evans, D. B.; Spurgeon, J. M.; Warren, E. L.; Briggs, R. M.; Lewis, N. S.; Atwater, H. A., Si microwire-array solar cells. *Energy Environ. Sci.* **2010,** *3*, 1037-1041, DOI.
- 22. Boettcher, S. W.; Warren, E. L.; Putnam, M. C.; Santori, E. A.; Turner-Evans, D.; Kelzenberg, M. D.; Walter, M. G.; McKone, J. R.; Brunschwig, B. S.; Atwater, H. A.; Lewis, N. S., Photoelectrochemical Hydrogen Evolution Using Si Microwire Arrays. *J. Am. Chem. Soc.*2011, *133*, 1216-1219, DOI 10.1021/ja108801m.
- 23. Spurgeon, J. M.; Boettcher, S. W.; Kelzenberg, M. D.; Brunschwig, B. S.; Atwater, H. A.; Lewis, N. S., Flexible, Polymer-Supported, Si Wire Array Photoelectrodes. *Adv. Mater.*2010, *22*, 3277-3281, DOI.
- 24. Shaner, M. R.; McDowell, M. T.; Pien, A.; Atwater, H. A.; Lewis, N. S., Si/TiO₂ Tandem-Junction Microwire Arrays for Unassisted Solar-Driven Water Splitting. *J. Electrochem. Soc.* **2016**, *163*, H261-H264, DOI 10.1149/2.0141605jes.
- 25. Chakthranont, P.; Hellstern, T. R.; McEnaney, J. M.; Jaramillo, T. F., Design and Fabrication of a Precious Metal-Free Tandem Core-Shell p(+)n Si/W-Doped BiVO₄ Photoanode for Unassisted Water Splitting. *Adv. Energy Mater.* **2017**, *7*, 1701515, DOI 10.1002/aenm.201701515.
- 26. Chen, C. T.; Turner-Evans, D. B.; Emmer, H.; Aloni, S.; Atwater, H. A.; Ieee In *Design* and *Growth of III-V on Si Microwire Array Tandem Solar Cells*, 39th IEEE Photovoltaic Specialists Conference (PVSC), Tampa, FL, Jun 16-21; Tampa, FL, 2013; pp 3397-3401.

- 27. Shaner, M. R.; Fountaine, K. T.; Ardo, S.; Coridan, R. H.; Atwater, H. A.; Lewis, N. S., Photoelectrochemistry of core-shell tandem junction n-p(+)-Si/n-WO₃ microwire array photoelectrodes. *Energy Environ. Sci.* **2014,** *7*, 779-790, DOI 10.1039/c3ee43048k.
- 28. Narkeviciute, I.; Chakthranont, P.; Mackus, A. J. M.; Hahn, C.; Pinaud, B. A.; Bent, S. F.; Jaramillo, T. F., Tandem Core-Shell Si-Ta₃N₅ Photoanodes for Photoelectrochemical Water Splitting. *Nano Lett.* **2016**, *16*, 7565-7572, DOI 10.1021/acs.nanolett.6b03408.
- 29. Kunturu, P. P.; Zachariadis, C.; Witczak, L.; Nguyen, M. D.; Rijnders, G.; Huskens, J., Tandem Si Micropillar Array Photocathodes with Conformal Copper Oxide and a Protection Layer by Pulsed Laser Deposition. *ACS Appl. Mater. Interfaces* **2019**, *11*, 41402-41414, DOI 10.1021/acsami.9b14408.
- 30. Gulati, S.; Mulvehill, M. C.; Pishgar, S.; Spurgeon, J. M., In Situ Magnetic Alignment of a Slurry of Tandem Semiconductor Microwires Using a Ni Catalyst. *Small* **2022**, *18*, 2103822, DOI 10.1002/smll.202103822.
- 31. Kelzenberg, M. D.; Boettcher, S. W.; Petykiewicz, J. A.; Turner-Evans, D. B.; Putnam, M. C.; Warren, E. L.; Spurgeon, J. M.; Briggs, R. M.; Lewis, N. S.; Atwater, H. A., Enhanced absorption and carrier collection in Si wire arrays for photovoltaic applications. *Nature Mater*. **2010**, *9*, 239-244, DOI 10.1038/nmat2635.
- 32. Fountaine, K. T.; Atwater, H. A., Mesoscale modeling of photoelectrochemical devices: light absorption and carrier collection in monolithic, tandem, Si/WO₃ microwires. *Opt. Express* **2014,** *22*, A1453-A1461, DOI 10.1364/oe.22.0a1453.
- 33. Kempler, P. A.; Ifkovits, Z. P.; Yu, W. L.; Carim, A. I.; Lewis, N. S., Optical and electrochemical effects of H₂ and O₂ bubbles at upward-facing Si photoelectrodes. *Energy Environ. Sci.* **2021**, *14*, 414-423, DOI 10.1039/d0ee02796k.

- 34. Liu, B.; Aydil, E. S., Growth of Oriented Single-Crystalline Rutile TiO₂ Nanorods on Transparent Conducting Substrates for Dye-Sensitized Solar Cells. *J. Am. Chem. Soc.* **2009**, *131*, 3985-3990, DOI 10.1021/ja8078972.
- 35. Bora, L. V.; Mewada, R. K., Visible/solar light active photocatalysts for organic effluent treatment: Fundamentals, mechanisms and parametric review. *Renew. Sust. Energ. Rev.* **2017**, 76, 1393-1421, DOI 10.1016/j.rser.2017.01.130.
- 36. Convertino, A.; Maiolo, L.; Scuderi, V.; Di Mauro, A.; Scuderi, M.; Nicotra, G.; Impellizzeri, G.; Fortunato, G.; Privitera, V., A forest of SiO₂ nanowires covered by a TiO₂ thin film for an efficient photocatalytic water treatment. *RSC Adv.* **2016**, *6*, 91121-91126, DOI 10.1039/c6ra15986a.
- 37. Rochkind, M.; Pasternak, S.; Paz, Y., Using Dyes for Evaluating Photocatalytic Properties: A Critical Review. *Molecules* **2015**, *20*, 88-110, DOI 10.3390/molecules20010088.
- 38. Xu, C.; Rangaiah, G. P.; Zhao, X. S., Photocatalytic Degradation of Methylene Blue by Titanium Dioxide: Experimental and Modeling Study. *Ind. Eng. Chem. Res.* **2014**, *53*, 14641-14649, DOI 10.1021/ie502367x.
- 39. Hou, L. R.; Yang, L.; Li, J. Y.; Tan, J.; Yuan, C. Z., Efficient Sunlight-Induced Methylene Blue Removal over One-Dimensional Mesoporous Monoclinic BiVO₄ Nanorods. *J. Anal. Methods Chem.* **2012**, *2012*, 345247, DOI 10.1155/2012/345247.
- 40. Khan, I.; Saeed, K.; Zekker, I.; Zhang, B. L.; Hendi, A. H.; Ahmad, A.; Ahmad, S.; Zada, N.; Ahmad, H.; Shah, L. A.; Shah, T. R.; Khan, I., Review on Methylene Blue: Its Properties, Uses, Toxicity and Photodegradation. *Water* **2022**, *14*, 242, DOI 10.3390/w14020242.

- 41. Spurgeon, J. M.; Atwater, H. A.; Lewis, N. S., A comparison between the behavior of nanorod array and planar Cd(Se, Te) photoelectrodes. *J. Phys. Chem. C* **2008**, *112*, 6186-6193, DOI 10.1021/jp077481u.
- 42. Haussener, S.; Xiang, C. X.; Spurgeon, J. M.; Ardo, S.; Lewis, N. S.; Weber, A. Z., Modeling, simulation, and design criteria for photoelectrochemical water-splitting systems. *Energy Environ. Sci.* **2012**, *5*, 9922-9935, DOI 10.1039/c2ee23187e.
- 43. El Yousfi, A.; Bouda, H.; El Hachimi, A. G.; Arshad, M. A.; El Kenz, A.; Benyoussef, A., Enhanced optical absorption of rutile TiO₂ through (Sm, C) codoping: a first-principles study. *Opt. Quantum Electron.* **2021,** *53*, 95, DOI 10.1007/s11082-021-02735-z.

TOC IMAGE

